

Predicting the Structural Performance of the Wings of an Unmanned Aircraft Vehicle Using Fluid-structure Interaction

K. Marangi, Salim M. Salim

ABSTRACT— This study combines computational fluid dynamics (CFD) and finite element analysis (FEA) to predict the impact of a wind gust on the wings and the wing-fuselage connectors of an Unmanned Aircraft Vehicle (UAV). The wind gust is modelled as a sudden increase in airspeed, 10 m/s above the UAV cruise velocity of 13 m/s, and compared to normal wind conditions. For the CFD simulations, *Spalart-Allmaras* and *k- ω SST* are employed in ANSYS FLUENT and the numerical results validated against XFLR5 (a semi-empirical software based on Massachusetts Institute of Technology’s famous low Reynolds number CFD program, XFOIL). During the wind gust condition, the lift increases to 244 N and drag to 13.2 N compared to the normal wind condition of 77.2 N and 4.34 N, in lift and drag respectively. The CFD calculated aerodynamic loads were coupled to ANSYS MECHANICAL to determine the resulting structural response on the wings. The maximum stress was observed along a slender component connecting the back-wing’s spar and shell, with a magnitude of 23.8 MPa and 75.0 MPa for the normal and wind gust flight conditions, respectively. The numerically calculated stresses on the wings obtained from ANSYS MECHANICAL are then used to analytically predict the structural response of the wing-fuselage connectors. The investigation, on the aerodynamic loads and resulting mechanical stresses produced in the wings and transferred to the wing-fuselage connectors, identified that despite an increase in loading during wind gust condition, the resulting stresses are still way below the critical levels.

Keywords— Aerodynamic loads, CFD, fluid-structure interaction, turbulence, UAV

I. INTRODUCTION

The structural performance of a UAV’s wings is investigated by using a one-way FSI analysis by coupling CFD and FEA, for two flight conditions: comparing airspeed of 13 m.s⁻¹ (*normal* flight condition) to airspeed of 23 m.s⁻¹ (*wind gust* flight condition). Table I summarises the inlet velocities in addition to the materials used in the wings and in the wing-fuselage connectors. The wings are made of composite materials, whereas the back-wing’s wing-fuselage connectors are composed of PETG 3D printed parts, clamped with aluminium nutted bolts (Fig. 1).

Manuscript received 6th April 2019; revised 10th April 2019.
Participation at the conference was supported in part by the Institution of Mechanical Engineers (IMechE).

K. Marangi is a student with the Department of Mechanical Engineering, School of Science and Engineering, University of Dundee, DD1 4HN, Dundee, UK (Phone: +447481978887; e-mail: k.marangi@dundee.ac.uk).

Dr. S. M. Salim *CEng MIMechE* is with the School of Science and Engineering, University of Dundee, DD1 4HN, Dundee, UK (Phone: +44 (0) 1382 381378; e-mail: m.s.salim@dundee.ac.uk).

TABLE I. PARAMETERS USED IN PRESENT STUDY

Parameter	Value
Airspeed (ms ⁻¹)	13 (<i>normal-state</i>) ^a 23 (<i>wind gust</i>)
Wings’ materials ^a	Woven and unidirectional Carbon Fibre Reinforced Plastic; woven fibre glass and epoxy resin; EPP foam
Wing-fuselage connector’s materials ^a	PETG (3D printed); aluminium alloy bolt

^aValues for normal inlet velocity, materials present in the wings & connector are obtained from the student team (Haggis Aerospace) in charge of the UAV [1], but data owned by the author K. Marangi.

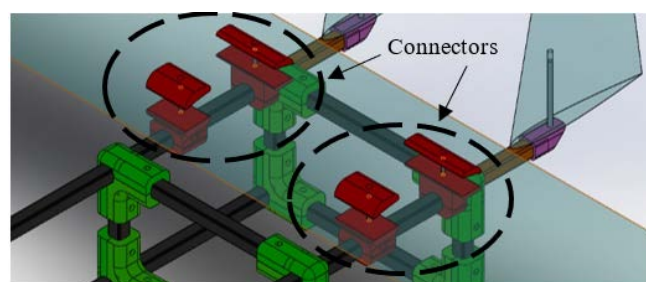


Fig. 1. Close-up view of the components connecting the back-wing and the fuselage.

The present study’s UAV CAD model is presented in Fig. 2, which features a non-traditional wing configuration. Instead of placing the smaller flying surfaces behind the larger wing as found in conventional aircrafts, the order is reversed. This special arrangement is referred to as a “lifting canard wing configuration”, implying that both canard wings and back-wing generate lift, as opposed to the entire lift being exclusively generated by the large wing in a conventional wing setup.

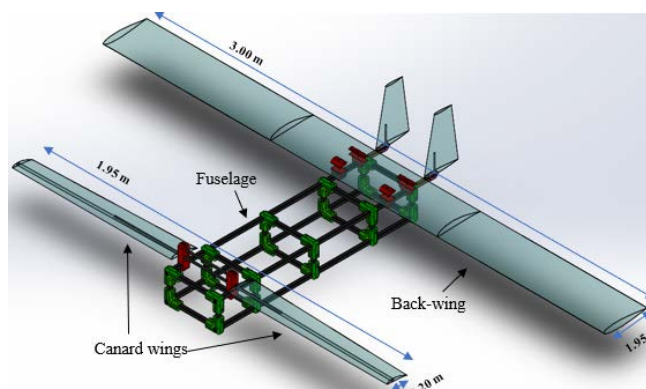


Fig. 2. Present Study’s Computer-Aided Design (CAD) model.

CFD simulations are first carried out to determine the

aerodynamic loads on the wings. These loads are exported to ANSYS MECHANICAL to evaluate the resulting forces. Finally, the numerically calculated stresses on the wings are exported to analytically resolve the stresses on the wing-fuselage connector. The work-flow for the present investigation is illustrated in Fig. 3.

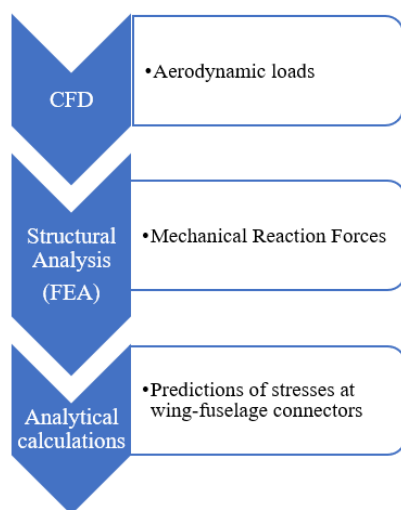


Fig. 3. Present study's work-flow.

P. Panagiotou *et al.* [2] employed the *Spalart-Allmaras* (SA) turbulence model, whereas S. Kontogiannis *et al.* [3] used the *k- ω SST* turbulence model in previous CFD studies on aerodynamic considerations of UAVs. Both turbulence models are adequate for UAV applications, as SA was developed for aerospace applications [4] and *k- ω SST* performs impressively in transitional and low Reynolds number flows [5]. The present study implemented both turbulence models for the CFD part in order to assess their respective performance by comparing against validation data which is obtained using the open-source XFLR5 software.

In separate studies, G. Kanesan *et al.* [6] and M. Ramos [7], utilised FEA to investigate the structural performance of their UAV's wings. Considering that their wings' structural designs are similar to the current UAV design's in terms of materials used and boundary conditions, the present study adopted their methodology.

Results obtained from coupling CFD to FEA analysis provides an insight on the structural integrity of the UAV wings and wing-fuselage connectors under different flight conditions.

II. METHODOLOGY

A. Computational Domain and Boundary Conditions

In the absence of experimental data, validation was carried out by comparing the ANSYS CFD results with data produced by XFLR5. A. Deperrois' [8] and J. Morgado *et al.* [9] demonstrated that XFLR5 can be used as a viable alternative. XFLR5 performed very well when compared against experimental results, providing an adequate level of physical accuracy for low Reynolds numbers. Due to this, XFLR5 is often employed in industry for CFD analysis related to diverse UAVs applications to investigate and optimise the aerodynamic design of any airfoil-dependent

model [10].

A half-body computational domain is employed under the assumption of symmetry, as shown in Fig. 4.

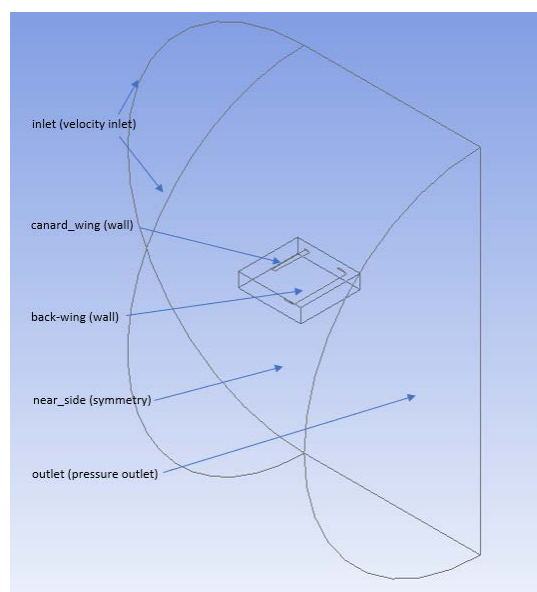


Fig. 4. Computational domain used in flow simulation of present study.

The computational domain comprised of approximately 3,000,000 cells (Fig. 5), using inflation layers with $y^+=1$, to ensure an adequate cell resolution for the boundary layer phenomena [2]-[3] and [11]-[12].

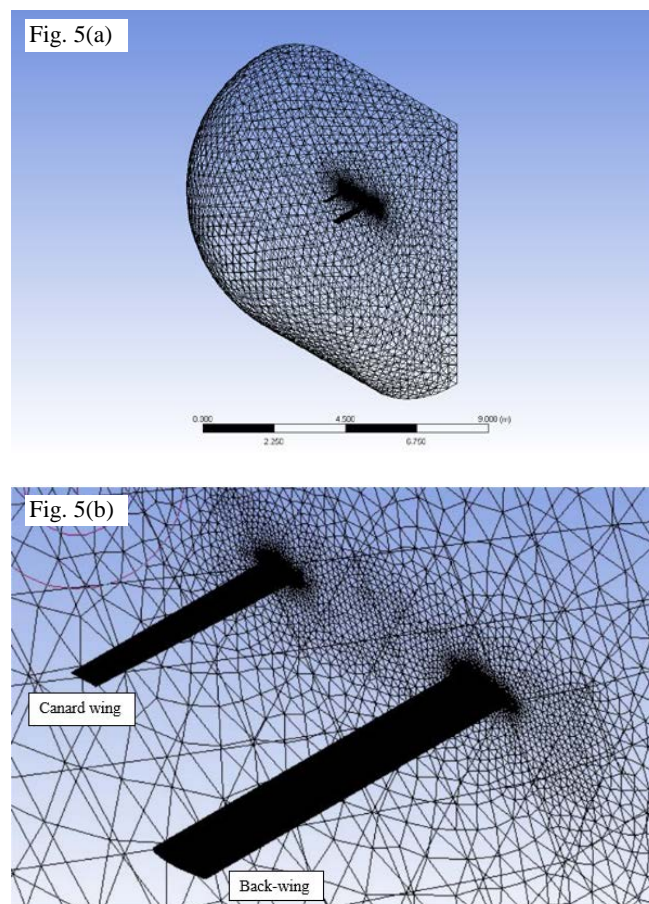


Fig. 5. CFD computational grid: (a) isometric view; (b) close-up view.

The boundary conditions used in the present simulations are summarised in Table II.

TABLE II. BOUNDARY CONDITIONS FOR FLOW SIMULATIONS

Boundary Name	Boundary Type	Conditions
Inlet	velocity inlet	$p = 0$ atm (gauge pressure); $T = 300$ K; $v_1 = 13$ m.s ⁻¹ (<i>normal state</i>); $v_2 = 23$ m.s ⁻¹ (<i>wind gust</i>); Angle of incidence = 3.0°
Near side	symmetry	Symmetrical with respect to boundary
Canard wing; Back-wing	wall	$v = 0$ m.s ⁻¹ (no-slip condition)
Outlet	pressure outlet	-

Two different inlet velocities are investigated corresponding to the two flight conditions of *normal* and *wind gust*, to predict whether the UAV would keep its structural integrity due to increase in airspeed.

B. Modelling of UAV Wing and Wing-fuselage Connectors

The back-wing's structural design consists of an EPP foam core shelled by a 3 mm thick laminated Glass-Fibre Reinforced Plastic (GRP). A Carbon-Fibre Reinforced Plastic (CFRP) tube runs through the wing's thickest part, which acts as the wing's spar (Fig. 6). Unidirectional CFRP bars connect the CFRP spar to the GRP shell in order to transmit any torsional moment produced from aerodynamic loading to the spar directly [13].

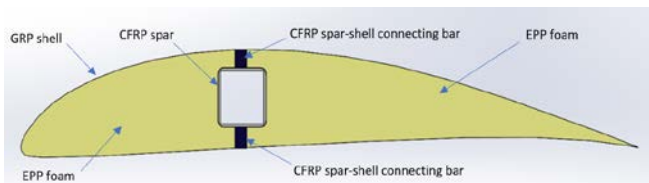


Fig. 6. Back-wing's wingroot cross-section – by Haggis Aerospace [1] but owned by the author K. Marangi.

Table III summarises the mechanical properties (Young's Modulus E (MPa) & Poisson's ratio ν in the three perpendicular directions) of the materials forming the wings, extracted from ANSYS' Material Library [14].

TABLE III. MECHANICAL PROPERTIES OF WINGS' MATERIALS

Parameter	Glass fibre Reinforced Plastic (woven, wet)	Carbon Fibre Reinforced Plastic (woven, wet)	Carbon Fibre Reinforced Plastic (UD, wet)
E_x (MPa)	35,000	59,160	$1.23 \cdot 10^5$
E_y (MPa)	9,000	59,160	7,780
E_z (MPa)	9,000	7,500	7,780
ν_{xy}	0.28	0.04	0.27
ν_{yz}	0.4	0.3	0.42
ν_{xz}	0.28	0.3	0.27

With respect to the modelling of the back wing's connectors, whose CAD models are shown in Fig. 2, it is necessary to make a few assumptions in calculating the resulting stress analytically. The connectors are composed of two elements: 3D-printed parts, and a M4 bolt, which provides clamping power to the overall component. To simplify this structural problem, the following assumptions are made:

- The front connectors are placed on top of the wing's neutral point (entire generated aerodynamic load is applied to this fixed region);
- As the nutted bolt is providing the clamping power in the connectors, the aerodynamic load is directly applied to these nutted bolts;
- Only the lift force is considered as the drag force is negligible in comparison;
- The mechanics of fasteners is not considered; therefore, assuming the bolt is homogeneous and isotropic; its stress limits [15], summarised in Table IV, are used to determine its structural integrity.

TABLE IV. MECHANICAL PROPERTIES OF THE BOLT'S ISOTROPIC MATERIAL (ALUMINIUM ALLOY)

Parameter	Value
Young's Modulus (GPa)	72
Yield Strength (MPa)	505

By taking these assumptions, the stress formula (1) is used to determine the tensile stress in the M4 bolt for each of the aerodynamic load resulting from the different flight conditions (where σ is the resulting stress [Pa], F is the applied force [N], & A the item's cross-sectional area [m²]).

$$\sigma = \frac{F}{A} \quad (1)$$

C. Numerical Setup

The SA and $k-\omega$ SST turbulence closure schemes are employed to predict the flow field around the UAV and the resulting pressure distribution representing the aerodynamic loads on the wings.

These loads obtained from flow simulations in FLUENT are then mapped onto the corresponding structural models in ANSYS MECHANICAL. Note that only half the body is evaluated due to the assumption of symmetry [6]-[7].

III. RESULTS AND DISCUSSIONS

A. Flow Simulation

The numerical results produced by the two turbulence schemes in FLUENT are compared and against values generated by XFLR5.

Tables V and VI present the resulting values for the aerodynamics loads, i.e. lift and drag forces, generated for the *normal* and *wind gust* flight conditions, respectively.

TABLE V. AERODYNAMIC LOADS: NORMAL CONDITION ($V=13$ MS⁻¹)

Parameter	Value	
Turbulence model	$k-\omega$ SST	SA
Lift force (N)	77.2	77.8
Drag force (N)	4.34	4.04

TABLE VI. AERODYNAMIC LOADS: WIND GUST ($V=23$ MS⁻¹)

Parameter	Value	
Turbulence model	$k-\omega$ SST	SA
Lift force (N)	244	246
Drag force (N)	13.2	13.2

For the *normal* flight condition (Table V), the lift force found is physically verified as it corresponds to a situation in which the UAV (in the case it has a mass of 6.9 kg, corresponding to 67.6 N) reaches level-flight, i.e. the two vertical opposing forces during flight, lift and weight, approximately cancel each other out. The total lift forces for the *normal* state flight condition are 77.2 N using *k- ω SST*, and 77.8 N using *SA*.

Table VI presents the total lift forces for the *wind gust* flight condition, with values of 244 N using *k- ω SST*, and of 246 N using *SA*. It is possible to observe the similarity in the aerodynamic loading values predicted by the two turbulence models, i.e. 0.78% difference in lift for *normal* flight condition and 0.82% for *wind gust* flight condition. This negligible difference between results from *SA* and *k- ω SST* implies that either turbulence scheme could be used as they performed similarly.

The lift increases by 217% when the airspeed rises from 13 m.s⁻¹ to 23 m.s⁻¹. This is expected as a change in velocity, which is a squared term in the lift formula (2) (where ρ is the air's density [Pa], v the airspeed [ms⁻¹], S the projected wing area [m²], and C_L the lift coefficient), will result in a large increase in lift.

$$L = \frac{1}{2} \rho v^2 S C_L \quad (2)$$

Table VII presents the aerodynamic coefficients obtained in both ANSYS and XFLR5. All three approaches predicted a drag coefficient value of 0.05, but there was a discrepancy of around 20% in the lift coefficients generated by ANSYS when compared to XFLR5's.

TABLE VII. AERODYNAMIC COEFFICIENTS FROM CFD SIMULATIONS

Parameter	Value		
	k- ω SST	SA	XFLR5 ^a
Lift Coefficient	0.96	0.97	0.76
Drag Coefficient	0.05	0.05	0.05

^aXFLR5 values obtained from the student team (Haggis Aerospace) in charge of the UAV [1]. Data owned by the author K. Marangi.

This part of the present study, comparing performance between *k- ω SST* and *SA* Reynold-Averaged Navier-Stokes (RANS) turbulence models, verify that both are equally suitable in the aerodynamic analysis of UAVs.

Fig. 7 demonstrates the pressure coefficients along the wings for the two flight conditions. These coefficients depict the relative pressures throughout a specific flow field, based on equation (3) (where C_p is the pressure coefficient, p the static pressure at a specific location [Pa], p_∞ the freestream static pressure [Pa], p_0 the freestream stagnation pressure [Pa], ρ_∞ the freestream fluid density [kg.m⁻³] & V_∞ the plane's velocity [m.s⁻¹]).

$$C_p = \frac{p - p_\infty}{\frac{1}{2} \rho_\infty V_\infty^2} = \frac{p - p_\infty}{p_0 - p_\infty} \quad (3)$$

Comparing Fig. 7(a) and 7(b), it is clear that the *wind gust* flight condition generates a larger lift force due to the larger pressure difference between the under & upper surfaces of the wings. This is further illustrated using pressure coefficient contours & 3D streamlines in Fig. 8.

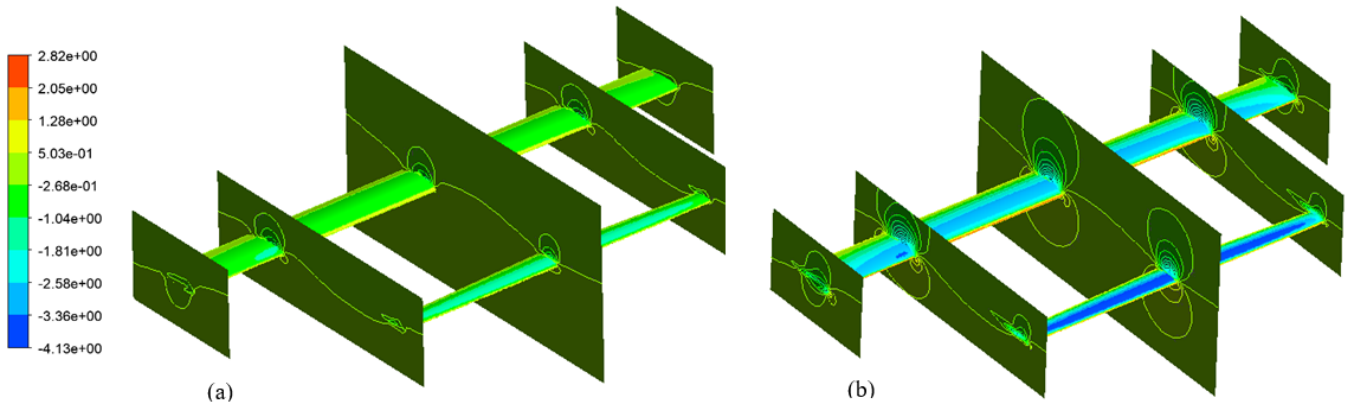


Fig. 7. Pressure Coefficient Contours (*k- ω SST*) for: (a) *normal* (13 ms⁻¹) and (b) *wind gust* (23 ms⁻¹) flight conditions.

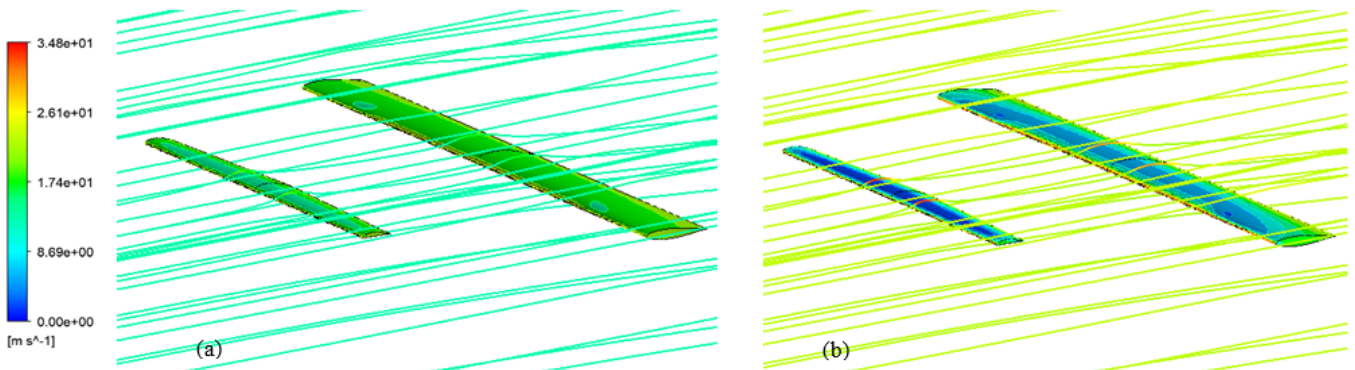


Fig. 8. 3D streamlines & Pressure Coefficient Contours (*k- ω SST*) for: (a) *normal* (13 ms⁻¹) and (b) *wind gust* (23 ms⁻¹) flight conditions.

The upper surface of the wing experiences a faster airspeed and consequently a lower air pressure, as opposed to the under surface. The observations agree with physical laws where the aerodynamic loads increase as a result of increased airspeed, i.e. during *wind gust* condition.

The next section will investigate the wings structural response to the generated aerodynamic loads to determine whether the components operate within reasonable safety margins.

B. Structural Analysis

The structural analysis consists of two steps: running the static structural simulation in ANSYS MECHANICAL and using the numerically obtained results to analytically resolve the stresses induced at the wing-fuselage connectors.

Table VIII presents the maximum stress, reaction force and maximum deformation experienced by both the canard and back wings for the *normal* and *wind gust* flight conditions, respectively.

TABLE VIII. RESULTS FROM FEA SIMULATIONS

Parameter	Value	
Wing	Canard	Back
Flight conditions	<i>Normal</i> ($v_1 = 13 \text{ ms}^{-1}$)	
Maximum Stress (MPa)	3.30	23.8
Reaction Force (N)	13.5	25.0
Maximum Deformation ($\cdot 10^{-3} \text{ m}$)	3.00	0.70
Flight conditions	<i>Wind gust</i> ($v_2 = 23 \text{ ms}^{-1}$)	
Maximum Stress (MPa)	10.0	75.0
Reaction Force (N)	42.2	78.9
Maximum Deformation ($\cdot 10^{-3} \text{ m}$)	9.50	2.25

As this study employs a static structural analysis, the location of maximum stresses on the wings remains unchanged regardless of the flight condition, only its magnitude changes according to different airspeeds. Fig. 9 presents the general locations of maximum equivalent stresses for each wing, although the overall maximum stress for both flight conditions is located on the back-wing. During *normal* flight condition, the back-wing's spar-shell connecting bar (Fig. 6) experiences stresses of a magnitude of 23.8 MPa and rising to 75.0 MPa during *wind gust* condition (Table VIII).

The present study uses a non-interactive theory [16], i.e. the maximum stress failure criteria, to determine the likelihood of a failure in the wings by evaluating the computed stresses against the material stress limits.

The stress is likely to be transmitted through bending, and given that bending consists of tensile and compressive stresses, it is a reasonable approximation to compare the obtained maximum equivalent stresses to the orthotropic stress limits in the relevant direction of bending. These are observed to be way below the tensile (1632 MPa) and compressive (-704 MPa) stress limits of the material (Table III).

Fig. 10 illustrates the wings' deformation in response to the aerodynamic load under both flight conditions. The largest deflection is located on the canard wing, with a value of 3.00 mm during *normal* condition, and increasing to 9.5 mm during *wind gust* condition (Table VIII) by a factor of 3. A possible reason causing this large deflection resides in the canard wing's design, which does not have any component connecting the spar to the GRP shell. Due to this, the aerodynamic load is not transmitted to the canard's spar, which results in the GRP shell experiencing the entire stresses from the canard's generated lift (Fig.9).

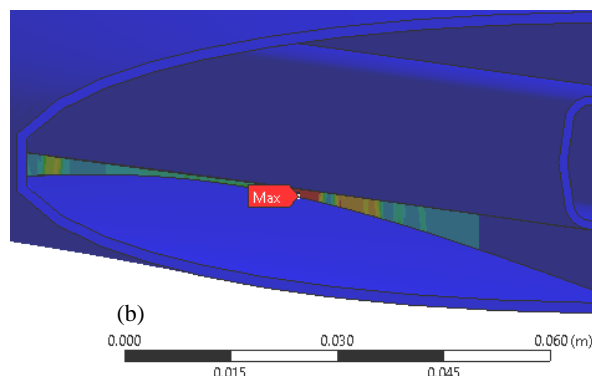
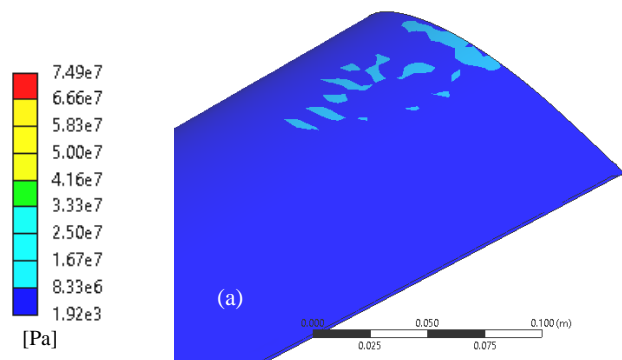


Fig. 9. Equivalent stress contours of (a) canard wing and (b) back-wing (close-up view on regions of high stresses for each wing).

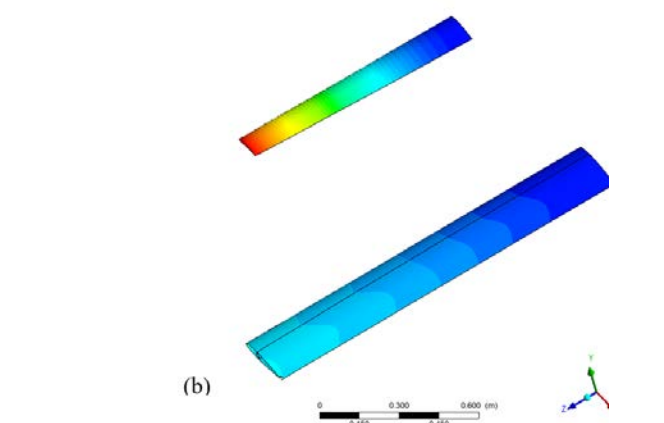
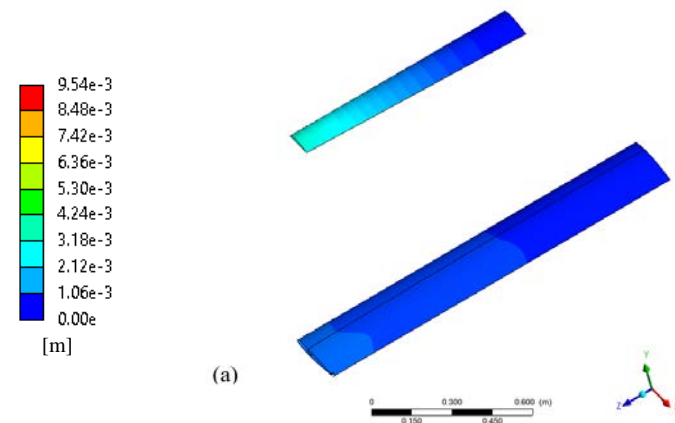


Fig. 10. Total deformation contours on wings for: (a) *normal* (13 ms^{-1}) and (b) *wind gust* (23 ms^{-1}) flight conditions.

Although the canard wings experience the largest deformation, the largest stresses are still located in the back-wing (Table VIII & Fig. 9 (b)).

The numerically computed results are used to analytically resolve the stresses transmitted to the wing-fuselage connector and presented in Table IX. During *normal* flight condition, it is predicted that the bolt will experience a tensile stress of 1.98 MPa, and raising to 5.95 MPa during *wind gust* condition, which is larger than the previous flight condition by a factor of 3. Fortunately, these are below the values of 505 MPa for the yield strength of the bolts implying that the Factor of Safety (FoS) is 85. The current connector design is sufficient and will not fail under the investigated flight conditions.

TABLE IX. RESULTS FROM ANALYTICAL ANALYSIS

Parameter	Value	
Flight condition	<i>Normal</i> ($v_1 = 13 \text{ ms}^{-1}$)	<i>Wind gust</i> ($v_2 = 23 \text{ ms}^{-1}$)
Cross-sectional area (m^2)	$1.26 \cdot 10^{-3}$	
Applied Force (N)	25.0	78.9
Resultant Stress (MPa)	1.98	5.95

IV. CONCLUSION

The present study investigates the structural integrity of UAV wings and wing-fuselage connector subjected to aerodynamic loading during two flight conditions. The airflow around the wings is first simulated using ANSYS FLUENT, and the resulting pressure fields imported into ANSYS MECHANICAL to undertake static structural analysis. The deflection and stresses experienced by the wings during the two flight conditions are numerically predicted. Finally, assumptions are made to analytically resolve the stresses experienced by the back-wing's wing-fuselage connector.

It was determined that during *wind gust* condition, the pressure difference between the wings' upper and lower surfaces is much larger than during *normal* condition as a result of the increased airspeed. Consequently, the amount of lift generated by the wings increased as well, producing larger stresses and deformations (by a factor of 3). Despite the increased loading and subsequently higher stresses, these were still below the limits by a safe margin.

ACKNOWLEDGEMENT

We thank the University of Dundee's "IMechE UAS Challenge" team HAGGIS AEROSPACE and Dr. Triantafyllos Gkikopoulos (RaptorUAS) for suggesting this research title and for the insightful discussions on UAVs.

REFERENCES

[1] Haggis Aerospace, *Critical Design Review*, document submitted for IMechE UAS Competition 2017, Dundee, 2017.
 [2] P. Panagiotou, P. Kaparos, C. Salpingidou and K. Yakinthos, "Aerodynamic design of a MALE UAV." *Aerospace Science and Technology*, vol. 50, pp.127-138, 2016.
 [3] S. Kontogiannis, D. Mazarakos and V. Kostopoulos, "ATLAS IV wing aerodynamic design: From conceptual approach to detailed optimization." *Aerospace Science and Technology*, vol. 56, pp.135-147, 2016.
 [4] P. Spalart and S. Allmaras, "A one-equation turbulence model for aerodynamic flows", *30th Aerospace Sciences Meeting and Exhibit*, 1992.

[5] S. Kontogiannis and J. Ekaterinaris, "Design, performance evaluation and optimization of a UAV", *Aerospace Science and Technology*, vol. 29, no. 1, pp. 339-350, 2013.
 [6] G. Kanesan, S. Mansor and A. Abdul-Latif, "Validation of UAV Wing Structural Model for Finite Element Analysis", *Jurnal Teknologi*, vol. 71, no. 2, 2014.
 [7] M. Ramos, "Construction and Analysis of a Lightweight UAV Wing Prototype", M.S thesis, Técnico Lisboa, Lisbon, Portugal, 2015.
 [8] A. Deperrois, 2009, *About XFLR5 calculations and experimental measurements*. [ebook] Available: http://www.xflr5.com/docs/Results_vs_Prediction.pdf
 [9] J. Morgado, R. Vizinho, M. Silvestre and J. Páscoa, "XFOIL vs CFD performance predictions for high lift low Reynolds number airfoils", *Aerospace Science and Technology*, vol. 52, pp. 207-214, 2016.
 [10] "XFLR5", *Xflr5.com*, 2018. [Online]. Available: <http://www.xflr5.com/xflr5.htm>. [Accessed: 02- Nov- 2017].
 [11] S. M. Salim and S. C. Cheah, "Wall y+ Strategy for Dealing with Wall-bounded Turbulent Flows", *Proceedings of International MultiConference of Engineers and Computer Scientists*, vol.2, pp. 2165 – 2170, 2009.
 [12] S.M.Salim, M. Ariff and S. C. Cheah, "Wall y+ Approach for Dealing with Turbulent Flows over a Wall Mounted Cube", *Progress in Computational Fluid Dynamics*, vol. 10 (5-6), pp. 341 – 351, 2010.
 [13] M. Simons, *Aerodynamics of model aircraft flight*. 5th ed. Dorset, England: Special Interest Model Books Ltd, 2015.
 [14] WORKENCH MECHANICAL. ANSYS.
 [15] "Aluminium Socket Cap Bolt M4 x (0.7mm) x 20mm", *Pro-bolt.com*, 2015. [Online]. Available: <https://www.pro-bolt.com/aluminium-allen-bolt-m4-x-0-7mm-x-20mm-21.html>. [Accessed: 05- Mar- 2018].
 [16] N. Tiwari, 2018, *Introduction to Composite Materials and Structures: Strength of a Composite Lamina*. [ebook] Available: <https://nptel.ac.in/courses/112104168/L32.pdf>